The FEBS Journal

FEBS PRESS science publishing by scientists

The complete absence of cytoplasmic γ-actin results in no discernible phenotype in mice or primary fibroblasts

Lauren J. Sundby[1], Katelin M. Hawbaker[2], Jacob Powers[3], William M. Southern[3], Erynn E. Johnson[3], Xiaobai Patrinostro[3], Benjamin J. Perrin[2] and James M. Ervasti[3]

1 Program in Molecular, Cellular, Developmental Biology, and Genetics, University of Minnesota, Minneapolis, MN, USA
2 Department of Biology, Indiana University – Indianapolis, Indianapolis, IN, USA
3 Department of Biochemistry, Molecular Biology, and Biophysics, University of Minnesota, Minneapolis, MN, USA

Keywords
γ-actin; *Actg1*; actin; stereocilia

Correspondence
J. Ervasti, University of Minnesota, 6-155 Jackson Hall, 321 Church Street SE, Minneapolis, MN 55455, USA
Tel: 612-626-6517
E-mail: jervasti@umn.edu
and
B. Perrin, Department of Biology, Indiana University – Indianapolis, SL336, 723 W. Michigan St, Indianapolis, IN 46202, USA
Tel: 317-278-5717
E-mail: bperrin@iu.edu

(Received 25 August 2024, revised 26 December 2024, accepted 6 February 2025)

doi:10.1111/febs.70075

Mice and primary fibroblasts derived from mouse embryos completely lacking cytoplasmic β-actin, because the *Actb* gene was engineered to instead express γ-actin protein, have previously been found to be virtually devoid of phenotype. Here, we report the characterization of mice and mouse embryonic fibroblasts homozygous for an *Actg1* allele edited to translate β-actin instead of γ-actin (*Actg1*-coding beta; $Actg1^{c\text{-}b/c\text{-}b}$), which resulted in mice and fibroblasts that are devoid of γ-actin. We demonstrate that these $Actg1^{c\text{-}b/c\text{-}b}$ mice present with no measurable phenotype in survival, body mass, activity, muscle contractility, or auditory function. Primary fibroblasts derived from $Actg1^{c\text{-}b/c\text{-}b}$ mouse embryos were still proliferative, with several measured parameters of cell motility not different from wild type. From these and previous data, we conclude that β- and γ-actin proteins are redundant in primary embryonic fibroblasts and during normal mouse development.

Introduction

Actin is a ubiquitous protein involved in many important cell and tissue functions, including migration, cytokinesis, muscle contraction, structural support, and regulation of gene expression [1]. The many functions of actin are supported by a family of closely related proteins, or isoforms, that are expressed from six distinct genes in mammals. As a key component of many essential cellular processes, it is not surprising that mutations in the genes encoding actin are causative of many diseases in humans, such as severe developmental conditions, skeletal muscle myopathies, and progressive deafness [2–7].

The two ubiquitously expressed actins, cytoplasmic β- and γ-actin, share 99% amino acid sequence identity, and their respective genes, *Actb* and *Actg1*, share 89% identity in their coding sequences in mice [8]. Despite the high sequence similarity between the two cytoplasmic actins, an array of biochemical, cell biologic, and genetic data published over the last 4 decades have led to the generally accepted hypothesis that β- and γ-actin each support essential and non-redundant functions in cells and organisms. In direct contradiction to this hypothesis, however, we and others [9,10] used different gene editing

Abbreviations
ABR, auditory brainstem response; $Actb^{c\text{-}g}$, *Actb*-coding γ-actin; $Actg1^{c\text{-}b}$, *Actg1*-coding β-actin; MEFs are, mouse embryonic fibroblasts; MRTF-A, myocardin-related transcription factor A; SRF, serum response factor; TAZ, transcriptional coactivator with PDZ binding motif; WT, wild type; YAP, Yes-associated protein.

technologies to generate mice that expressed γ-actin protein from *Actb*, establishing a β-actin protein specific knockout that maintains an intact *Actb* nucleotide sequence, named $Actb^{c\text{-}g}$. The $Actb^{c\text{-}g}$ mice were largely phenotypically normal with no defect in survival [9,10]. $Actb^{c\text{-}g}$ mouse embryonic fibroblasts (MEFs) also had normal proliferation rates and migration patterns [9,10]. These and subsequent results [11] demonstrated that it is not the loss of β-actin protein that causes the most severe phenotypes in *Actb* knockout mice and MEFs, but rather the loss of a functional *Actb* gene locus.

Despite the nearly complete absence of phenotype in mice and MEFs lacking β-actin protein [9–11], highly specialized cell types, including auditory sensory hair cells and photoreceptors, degenerate in aging mice [10,12]. Thus, in some very specific circumstances, β-actin seems to have some function that is not also performed by γ-actin. To determine if γ-actin also has functions that cannot be fulfilled by β-actin, we generated mice and MEFs where the *Actg1* nucleotide sequence has been edited to express cytoplasmic β-actin instead of γ-actin. We report here the complete absence of detectable phenotype in the resulting mice and cells, which were devoid of γ-actin protein. Together with previous studies, we conclude that the 99% identical β-actin and γ-actin proteins are interchangeable in primary embryonic fibroblasts and during normal mouse development.

Results

$Actg1^{c\text{-}b/c\text{-}b}$ mice are overtly normal

Mice expressing β-actin from the *Actg1* gene (Fig. 1A), generated using CRISPR/Cas9 gene editing, were named $Actg1^{c\text{-}b}$ for *Actg1*-coding **b**eta to be consistent with the names of 2 mouse lines where *Actb* was gene edited to express γ-actin [9,10]. Four heterozygous $Actg1^{c\text{-}b/+}$ founder mice were generated and verified that *Actg1* exon2 encoded D2–4 and V10 of β-actin instead of E2–4 and I10 of γ-actin protein (Fig. 1B). While previous studies revealed that mice homozygous for *Actg1* alleles deleted for exons 2–3 have increased perinatal lethality [13], homozygous $Actg1^{c\text{-}b/c\text{-}b}$ mice were born in normal Mendelian ratios (27.9% $Actg1^{+/+}$, 51.7% $Actg1^{c\text{-}b/+}$, and 20.4% $Actg1^{c\text{-}b/c\text{-}b}$) and showed survival out to 180 days that was not different from control $Actg1^{+/+}$ littermates (Fig. 1C,D). The *Actg1* nucleotide sequence has been implicated in promoting normal mouse development and growth [13,14]. Here, we observed average body masses in both male and female $Actg1^{c\text{-}b/c\text{-}b}$ mice that were not different from WT (Fig. 1E,F). $Actg1^{c\text{-}b/c\text{-}b}$ mice displayed no defects in muscle contractile function, despite expressing no γ-actin protein (Fig. 2) and behaved normally in an open-field activity assay (Fig. 3). Together, these data suggest that the edits made to the *Actg1* locus did not negatively impact mouse viability. Taken in conjunction with previous studies that have shown that loss of *Actg1* impairs mouse survival and development [13,14] these data support previous conclusions that an intact *Actg1* gene, and not γ-actin protein, is necessary for normal mouse development and survival.

Verification of γ-actin protein ablation in $Actg1^{c\text{-}b/c\text{-}b}$ mice and MEFs

We measured isoactin transcript and protein expression in $Actg1^{c\text{-}b/c\text{-}b}$ mice to verify the absence of γ-actin protein and determine how editing *Actg1* to express β-actin alters the expression of other actin isoforms. Using qRT-PCR and primers specific to both the native and edited cytoplasmic actin transcripts, we observed a significant decrease in the native *Actg1* transcript in heterozygous $Actg1^{c\text{-}b/+}$ brain and lung tissue, and in MEFs, that was absent in homozygous $Actg1^{c\text{-}b/c\text{-}b}$ tissue with a concomitant increase in the edited $Actg1^{c\text{-}b}$ transcript (Fig. 4). Quantitative western blot analysis demonstrated that γ-actin protein was completely absent in $Actg1^{c\text{-}b/c\text{-}b}$ brain, lung, and MEFs, while β-actin expression significantly increased in the brain, trended higher in MEFs, but not in lung (Fig. 5). Tissue from $Actg1^{c\text{-}b/c\text{-}b}$ brain and lung showed a significant decrease in expression of endogenous *Actb* transcript (Fig. 4A,B), suggesting that some cell types have a mechanism to sense β-actin concentration to regulate *Actb* gene expression. Total actin levels were not different between WT and $Actg1^{c\text{-}b/c\text{-}b}$ in brain, lung, or MEFs (Fig. 5). We did not quantify actin levels in skeletal muscle (Fig. 2A) because β- and γ-actin cannot be measured in whole muscle lysates by western blotting due to the >4000-fold excess of skeletal α-actin that necessitates centrifugal separation and enrichment by DnaseI affinity chromatography for their detection [15,16].

$Actg1^{c\text{-}b/c\text{-}b}$ MEFs display normal parameters of cell motility

Previous data has demonstrated that random cell migration requires the *Actb* gene sequence but not β-actin, *Actg1*, or γ-actin [10,14,17,18]. To verify these previous results, we assessed random cell migration in MEFs harvested from $Actg1^{c\text{-}b/c\text{-}b}$ embryos.

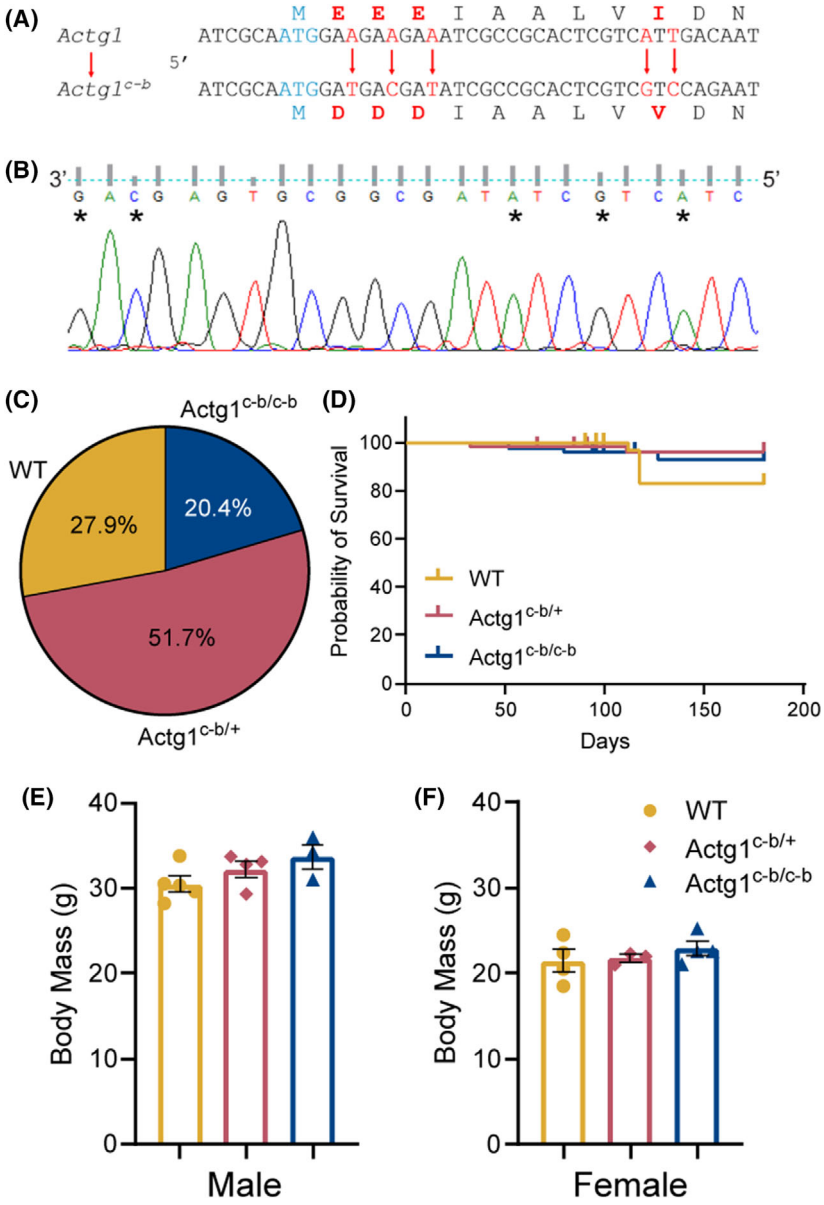

Fig. 1. *Actg1*$^{c\text{-}b/c\text{-}b}$ mice have similar birth rates, growth, and survival compared to control littermates. (A) Proposed sequence edits to mutate the wild type (WT) *Actg1* sequence to the new *Actg1*$^{c\text{-}b}$ sequence. (B) Sanger sequencing for a confirmed *Actg1*$^{c\text{-}b/c\text{-}b}$ mouse. Asterisks indicate successfully edited nucleotides. (C) Birth rates for WT ($n = 36$), *Actg1*$^{c\text{-}b/+}$ ($n = 56$), and *Actg1*$^{c\text{-}b/c\text{-}b}$ ($n = 50$) born from heterozygote *Actg1*$^{c\text{-}b/+}$ × *Actg1*$^{c\text{-}b/+}$ crosses. (D) Kaplan–Meier survival curve for WT, *Actg1*$^{c\text{-}b/+}$, and *Actg1*$^{c\text{-}b/c\text{-}b}$ from P0 to P180. Colored tick marks represent censored animals. Body mass for (E) male and (F) female mice at 3 months of age ($n \geq 3$). One-way ANOVA with Bonferroni posttest was performed. Error bars are SEM. Comparisons are not significant unless otherwise indicated.

Quantitation of distance traveled, individual cell paths, directionality, mean square displacement, and speed of *Actg1*$^{c\text{-}b/c\text{-}b}$ MEFs revealed no change in random migration habits (Fig. 6) suggesting that γ-actin protein is not required for cell migration. These data are in line with previous studies from our group [14,17].

The polymerization state of actin regulates the expression of a variety of genes via the serum response factor (SRF)/myocardin-related transcription factor (MRTF) signaling pathway [19–22]. To assess whether the altered expression of actin isoforms in *Actg1*$^{c\text{-}b/c\text{-}b}$ MEFs (Fig. 5C) influences the expression of key pathway regulators SRF and MRTF-A, we used quantitative western blot analysis to measure the expression of SRF and MRTF-A. While we note a significant increase in SRF immunoreactivity in *Actg1*$^{c\text{-}b/+}$ MEFs, we measured no significant change in either SRF or MRTF-A immunoreactivity in *Actg1*$^{c\text{-}b/c\text{-}b}$ MEFs relative to WT MEFs (Fig. 7). Additionally, actin plays a role in regulating the Hippo-Signaling pathway via transcriptional coactivator with PDZ binding motif (TAZ) and Yes-associated protein 1 (YAP, reviewed in [23]). However, quantitative western blotting of YAP expression in *Actg1*$^{c\text{-}b/c\text{-}b}$ MEFs showed no change in YAP expression relative to WT or *Actg1*$^{c\text{-}b/+}$ MEFs (Fig. 7). Together, these results suggest that neither the *Actg1*$^{c\text{-}b/c\text{-}b}$ genotype nor the absence of γ-actin protein impacts the SRF/MRTF or Hippo-Signaling

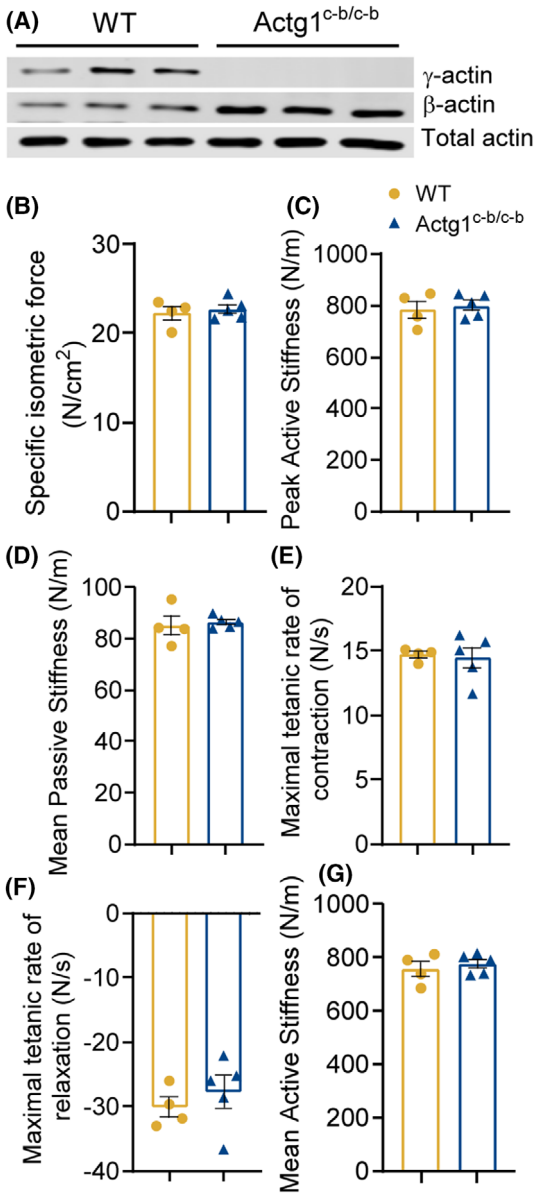

Fig. 2. *Actg1*$^{c\text{-}b/c\text{-}b}$ Muscle physiology does not differ from wild type. (A) Western blots of β-, γ-, and total Actin of Dnase-enriched gastrocnemius muscle from wild type (WT) and *Actg1*$^{c\text{-}b/c\text{-}b}$ mice ($n = 3$). (B) Specific isometric force, (C) passive stiffness, (D) mean passive stiffness, (E) maximum tetanic contraction rate, (F) maximum rate of tetanic relaxation, and (G) mean active stiffness of WT and *Actg1*$^{c\text{-}b/c\text{-}b}$ extensor digitorum longus (EDL) muscle. $n \geq 4$. Unpaired *t*-test was performed. Error bars are SEM. Comparisons are not significant unless otherwise indicated.

pathways. Because we previously measured a significant decrease in the G:F ratio of *Actb* KO MEFs [18], we measured the G:F ratio in *Actb*$^{c\text{-}g/c\text{-}g}$ MEFs but reported no difference compared to WT [10]. We previously measured no difference in G:F ratio between *Actg1* KO and WT MEFs [17]; therefore, we saw no reason to measure the G:F ratio in *Actg1*$^{c\text{-}b/c\text{-}b}$ MEFs here. We believe that the SRF/MRTF and YAP data support that there is no difference in actin dynamics between *Actg1*$^{c\text{-}b/c\text{-}b}$ and WT MEFs that would warrant the measurement of the G:F ratio in *Actg1*$^{c\text{-}b/c\text{-}b}$ MEFs.

Hearing function in *Actg1*$^{c\text{-}b/c\text{-}b}$ mice

Our previous studies demonstrated that *Actg1*$^{-/-}$ mice develop progressive hearing loss with concurrent degeneration of actin-rich stereocilia on auditory sensory hair cells by 16 weeks of age. We therefore tested auditory function in *Actg1*$^{c\text{-}b/c\text{-}b}$ mice by measuring auditory brainstem responses to pure tone sound stimuli ranging in frequency from 4 to 32 kHz. In contrast to what we observed in *Actg1* knockout mice, 16-week-old *Actg1*$^{c\text{-}b/c\text{-}b}$ mutants had similar or even slightly improved ABR thresholds, which correspond to the quietest sound that elicited a response, compared to age-matched control mice (Fig. 8A). Sound is converted to electrical signals by stereocilia, which are large protrusions that form around a core of β-actin and γ-actin filaments. Consistent with having unchanged ABR responses, *Actg1*$^{c\text{-}b/c\text{-}b}$ auditory outer hair cell stereocilia bundles retained a normal morphology characterized by the orderly arrangement of stereocilia into staircase-like rows (Fig. 8B). Thus, for at least 16 weeks in mice, γ-actin is dispensable for auditory hair cell development and maintenance.

Discussion

β- and γ-actins are generally redundant

An array of biochemical, cell biologic, and genetic data published over the last 40 years have generally supported the hypothesis that β- and γ-actin each support essential and non-redundant functions in cells and organisms. Our initial approach to define the essential isoform-specific functions of β- and γ-actin involved the generation of floxed mouse lines with loxP sites flanking exons 2 and 3 of *Actg1* and *Actb* to generate an array of mouse lines bearing whole body and tissue-specific knockouts of β-actin and γ-actin [5,13,17,18,24–27]. While our studies verified previous studies [28,29] demonstrating that the *Actb* gene is essential [18], we were surprised by the mild phenotypes manifest in tissue-specific *Actb* knockouts [5,25–27]. More surprisingly, whole body *Actg1* knockout mice were viable but with impaired growth and

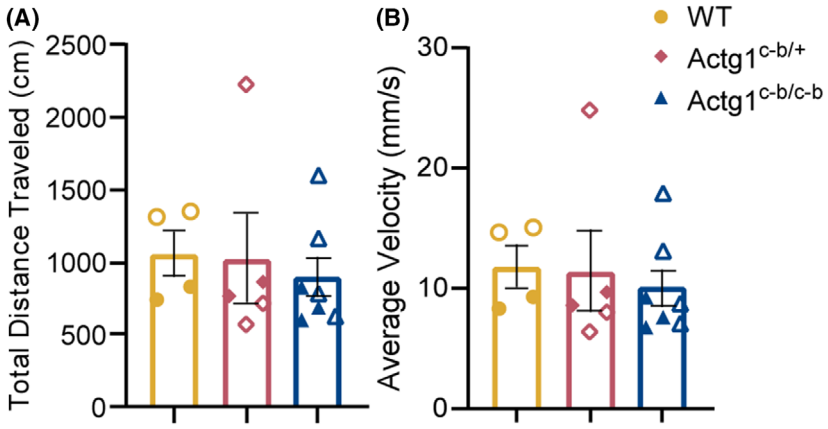

Fig. 3. *Actg1*$^{c\text{-}b/c\text{-}b}$ mice have wild-type activity levels. (A) Total horizontal distance traveled and (B) average velocity during a 15-min open-field activity assay on wild type (WT) ($n = 4$), *Actg1*$^{c\text{-}b/+}$ ($n = 5$), and *Actg1*$^{c\text{-}b/c\text{-}b}$ ($n = 7$) mice. Solid fill symbols represent males and open symbols represent females. One-way ANOVA with Bonferroni posttest was performed. Error bars are SEM. Comparisons are not significant unless otherwise indicated.

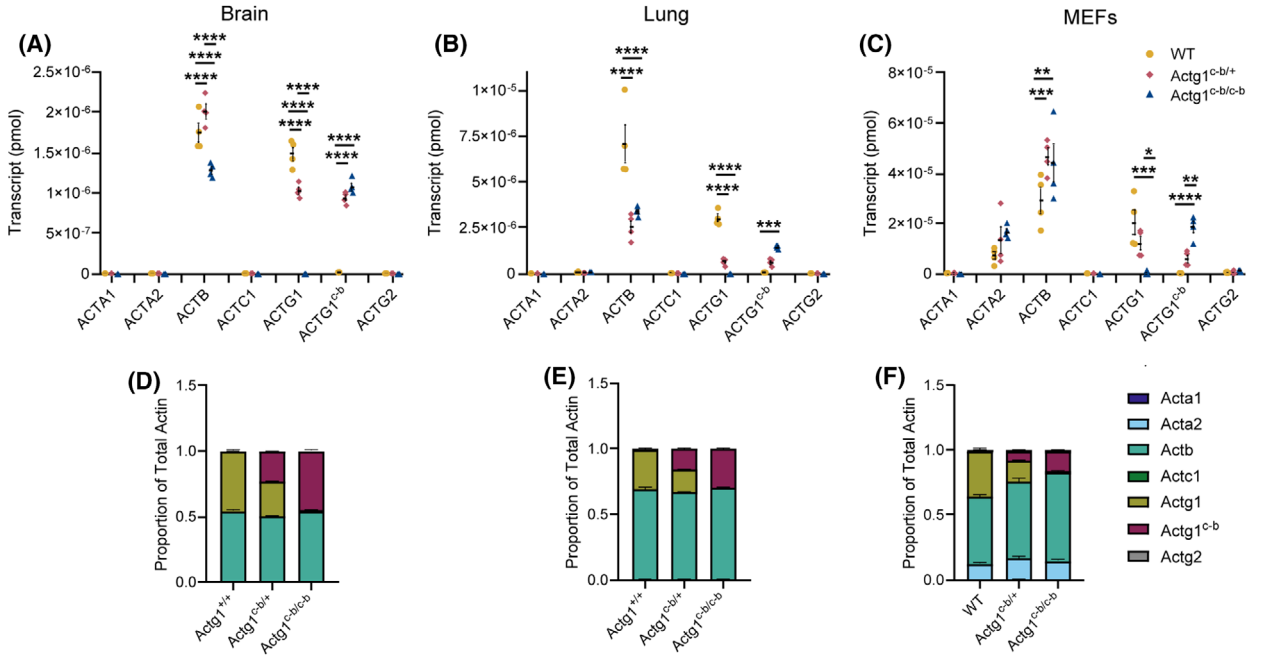

Fig. 4. *Actg1*$^{c\text{-}b}$ transcript is expressed from the edited *Actg1* gene. (A–C) Absolute and (D–F) proportional quantification of isoactin and *Actg1*$^{c\text{-}b}$ transcripts of wild type (WT), *Actg1*$^{c\text{-}b/+}$, and *Actg1*$^{c\text{-}b/c\text{-}b}$ brain, lungs, and mouse embryonic fibroblasts (MEFs) ($n = 4$, in triplicate). Transcript quantity was calculated using standard curves amplified in parallel. For A–C, two-way ANOVA with Bonferroni posttest was performed. $*P < 0.05$, $**P < 0.01$, $***P < 0.001$, $****P < 0.0001$. Error bars are SEM.

survival [13] and mild tissue-specific phenotypes [8,24]. Finally, against all expectations, we and others [9,10] found that mice engineered to express only γ-actin from both the *Actg1* and the *Actb* were largely phenotypically normal with no defect in survival. These and subsequent results [11] demonstrated that it is not the loss of β-actin that causes the most severe phenotypes in *Actb* knockout mice and MEFs, but rather the loss of a functional *Actb* gene locus. Contrasting with the findings of Patrinostro *et al.* (2018) and Vedula *et al.* (2017), some more recent *in vitro* studies in immortalized cancer cell lines have concluded that β- and γ-actin proteins have essential and non-redundant functions necessary for processes as fundamental as cytokinesis [30–35]. Here we importantly demonstrate the absence of detectable phenotype in mice and cells that are completely devoid of cytoplasmic γ-actin protein. When combined with the findings of Patrinostro *et al.* (2018) and Vedula *et al.* (2017), we conclude that β- and γ-actin proteins are redundant in primary embryonic fibroblasts and during normal mouse development.

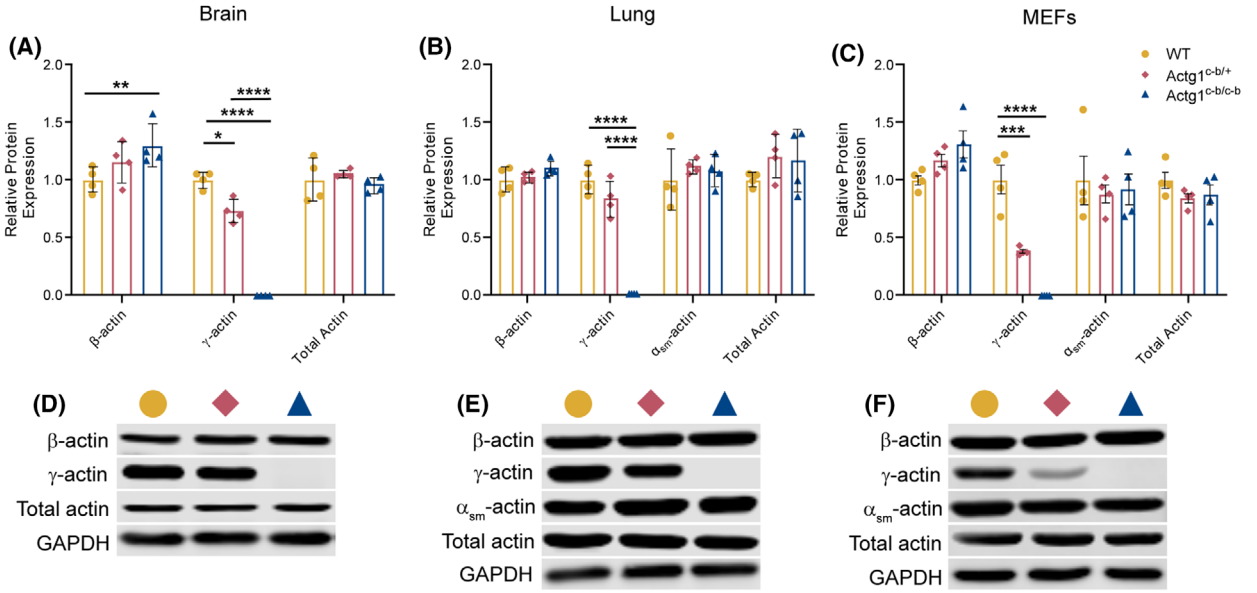

Fig. 5. *Actg1*$^{c\text{-}b/c\text{-}b}$ Mice express no γ-Actin protein. Relative Actin isoform protein expression in wild type (WT), *Actg1*$^{c\text{-}b/+}$, and *Actg1*$^{c\text{-}b/c\text{-}b}$ mice in (A) brain, (B) lungs, and (C) mouse embryonic fibroblasts (MEFs) ($n = 4$). The x-axis indicates Actin isoform and the y-axis represents relative protein expression normalized to GAPDH and relative to WT. Representative western blot images for each isoform in (D) brain, (E) lungs, and (F) MEFs. Two-way ANOVA with Bonferroni posttest was performed. *$P < 0.05$, **$P < 0.01$, ***$P < 0.001$, ****$P < 0.0001$. Error bars are SEM.

Highly specialized cell types are the exception to the rule

On the basis of gene disruption studies where exons 2 and 3 were removed by Cre-loxP mediated excision, we previously concluded that β- and γ-actin most likely had distinct, non-overlapping functions in stereocilia maintenance. This conclusion was borne out by the phenotype of the *Actb*$^{c\text{-}g}$ mouse, which lacks β-actin and, like the *Actb* deletion mouse, develops high-frequency hearing loss and exhibits concurrent degeneration of the shorter rows of stereocilia in outer hair cell bundles [10]. However, the result for the loss of γ-actin is different. Here, editing the *Actg1* gene to express β-actin protein did not result in any detectable auditory phenotype. These data suggest that γ-actin actually does not have any function in auditory hair cells that cannot be fulfilled by a sufficient amount of β-actin. Thus, in auditory hair cells, *Actg1* exists to supplement the actin pool while β-actin protein carries out some unique function for which γ-actin is insufficient.

Stereocilia are unique among characterized actin-based structures in that their actin core is exceptionally stable without detectable actin turnover along its length over a time course of several months in mice. Actin does turnover at stereocilia tips [36–38], and in this microenvironment where actin is made to behave strangely, it is understandable how very subtle differences between β-actin and γ-actin could matter over long time periods. Indeed, long-lived cellular structures may be a common thread to revealing essential roles for β-actin protein, as photoreceptor degeneration was also noted in older *Actb*$^{c\text{-}g}$ mice [12]. Other long-lived cells, such as neurons, have not been characterized in enough detail in these mutated actin mouse lines to detect potentially subtle differences that could nevertheless affect function.

Conclusion

The two exceptional circumstances where β-actin appears to be essential within the inner ear and retina [10,12] disprove the hypothesis that *Actb* and *Actg1* only serve to properly regulate the level of actin in cells. However, these same studies also demonstrate that mice lacking β-actin are born without an overt phenotype and live long enough to manifest only late-onset phenotypes, while our current study found no phenotype in mice lacking γ-actin. Our previous and current data thus disprove the hypothesis [32–34] that β-actin and γ-actin protein differences are essential for fundamental processes like cytokinesis in the context of primary embryonic fibroblasts and mouse development, but leave open the possibility that β-actin and γ-actin may perform more specific and unique functions in immortalized cancer cells.

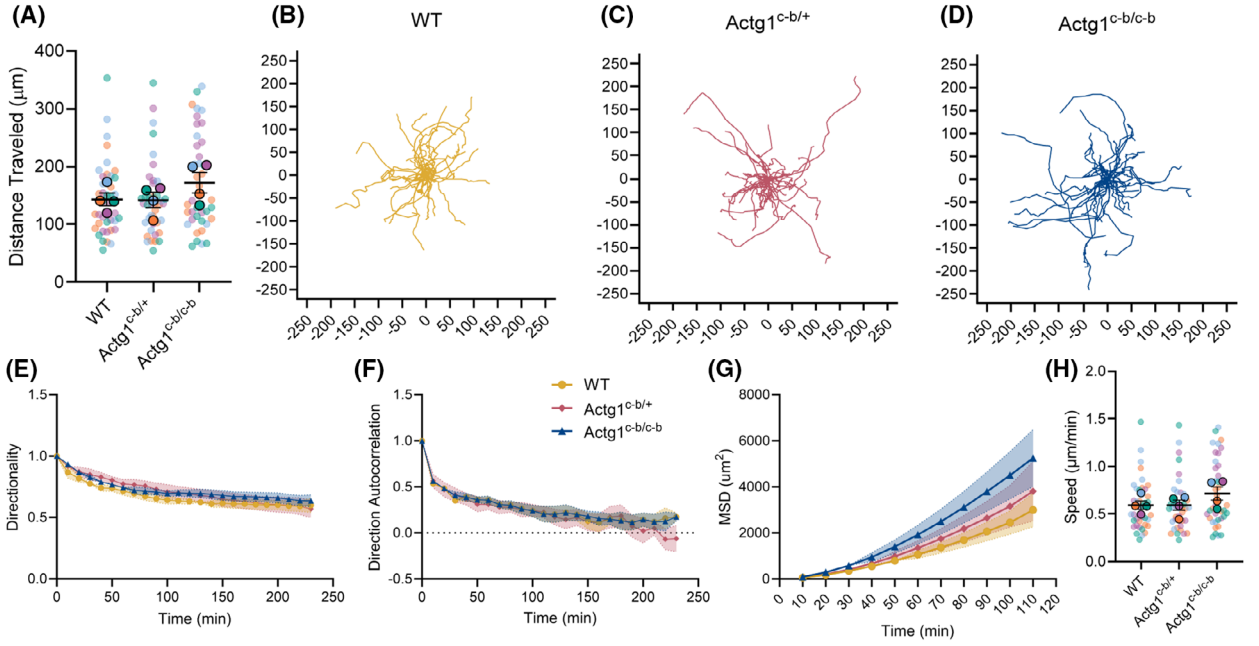

Fig. 6. Random cell migration is unchanged in *Actg1*$^{c\text{-}b/c\text{-}b}$ mouse embryonic fibroblasts (MEFs). (A) Total distance traveled and (B–D) paths traveled by individual cells mapped from the origin for wild type (WT), *Actg1*$^{c\text{-}b/+}$, and *Actg1*$^{c\text{-}b/c\text{-}b}$ MEFs. Each line corresponds to an independent cell. (E) Directionality, (F) directional autocorrelation, (G) mean square displacement and (H) speed of cells from each genotype. $N = 4$, $n = 10$ cells per embryo. For A and H, each color represents an independent experiment. Smaller circles represent the distance traveled or speed of each independent cell and larger bolded circles represent the means of each independent experiment. For E–G, two-way ANOVA with repeated measures and Bonferroni posttest was performed. For A and H, a one-way ANOVA with Bonferroni posttest was performed; statistical analysis was performed on the means of independent experiments. Error bars are SEM. Comparisons are not significant unless otherwise indicated.

Materials and methods

Mice

Animals were treated and housed in accordance with University of Minnesota Institutional Animal Care and Use Committee (IACUC) Standards. All experiments using animals were approved by the University of Minnesota IACUC under protocol number 2106-A39169. Mice were housed on a 12-hour light/dark cycle with *ad libitum* access to food and water in a specific pathogen-free facility. This study used male and female animals on the C57BL/6J background, with wild-type controls being littermates not carrying the edited allele. Mice were killed using cervical dislocation following anesthesia with Avertin at 3 months of age for all phenotypic analyses except hearing, which occurred at 16 weeks. Collected tissues were dissected and snap-frozen in liquid nitrogen.

Generation of *Actg1*$^{c\text{-}b}$ mKI mice model

Actg1$^{c\text{-}b/c\text{-}b}$ knock-in mice were generated by Biocytogen (Waltham, MA, USA) using a CRISPR/Cas9-based approach. Briefly, two sgRNAs were designed using a CRISPR design tool (http://www.sanger.ac.uk/) to target the region upstream of *Actg1* exon 2 and were then screened for on-target activity using a Universal CRISPR Activity Assay (UCA™; Biocytogen Pharmaceuticals). The T7 promoter sequence was added to the Cas9 or sgRNA template by PCR amplification *in vitro*. Variable concentrations of donor vector and purified *in vitro* transcribed Cas9 mRNA and sgRNAs were mixed and co-injected into the cytoplasm of single-cell stage fertilized eggs of C57BL/6N mice (Biocytogen). sgRNA1 (5′) – 5′-GCAGCCCCTCCTCGCCGCG GCGG-3′, sgRNA2 (3′) – 5′-ATGCCCGTTAGCAACTC AAGTGG-3′. The injected zygotes were transferred into the oviducts of Kunming pseudo-pregnant female mice to generate F0 mice. PCR and sequencing verification of founder pups harboring the intended mutation were then crossed with wild-type mice for germline transmission, which were further confirmed by PCR, sequencing, and Southern blot. Genotyping primers: *Actg1*$^{c\text{-}b}$ forward primer – 5′-TGAC GATATCGCCGCACTCGTCG-3′, *Actg1* exon 2 WT forward primer – 5′-AGAAGAAATCGCCGCACTCGTC ATT-3′, *Actg1*/*Actg1*$^{c\text{-}b}$ dual reverse primer – 5′-GGCAA GGTCCCGGCTCAAGC-3′. Sanger Sequencing was performed by the University of Minnesota Genomics Center (Minneapolis, MN, USA). PCR was performed using Taq

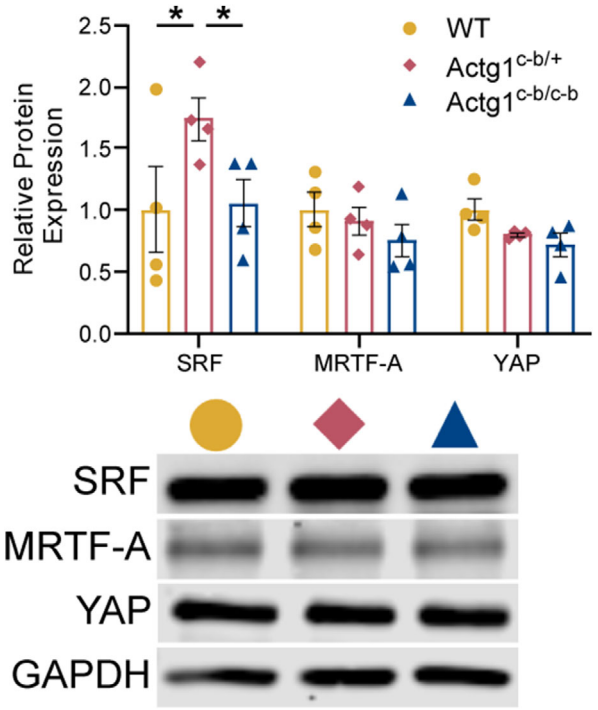

Fig. 7. Expression of select Actin-associated proteins is unchanged in *Actg1*$^{c\text{-}b/c\text{-}b}$ mouse embryonic fibroblasts (MEFs). Relative protein expression of Actin-associated proteins SRF, MRTF-A, and YAP normalized to GAPDH and relative to wild type (WT) in WT, *Actg1*$^{c\text{-}b/+}$, and *Actg1*$^{c\text{-}b/c\text{-}b}$ MEFs ($n = 4$). Two-way ANOVA with Bonferroni posttest was performed. *$P < 0.05$. Error bars are SEM.

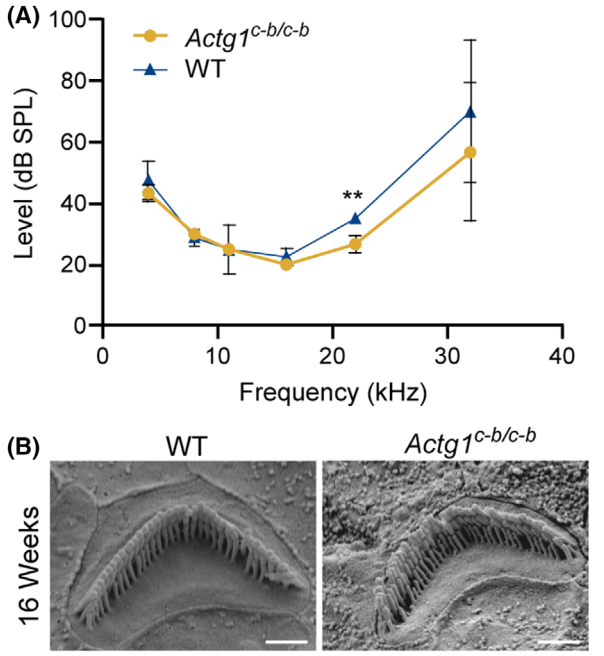

Fig. 8. Auditory brainstem response (ABR) and stereocilia morphology are unchanged in *Actg1*$^{c\text{-}b/c\text{-}b}$ mice. (A) ABR and (B) SEM images of 16 week-old wild type (WT) and *Actg1*$^{c\text{-}b/c\text{-}b}$ mice ($n \geq 3$). SEM images of cochlea middle turn OHC. Scale bar: 1 μm. X-axis indicates ABR defined frequency in kilohertz and y-axis indicates threshold (in decibels) sound that elicits a response. Student's T-test was performed. **$P < 0.01$. Error bars are SD. Comparisons are not statistically significant unless indicated otherwise.

DNA Polymerase and Standard Taq Buffer (#M0273S; New England BioLabs, Ipswich, MA, USA).

Cell culture

Primary WT, Actg1,$^{c\text{-}b/+}$, and Actg1$^{c\text{-}b/c\text{-}b}$ mouse embryonic fibroblasts (MEFs) were isolated from E13.5 embryos as previously described [17]. MEFs were cultured to approximately 80% confluency in DMEM supplemented with 10% fetal bovine serum, 1% Penicillin/Streptomycin, and 0.5 μg·mL^{-1} Fungizone (MEF media) and 1 × 10^6 MEFs were frozen at passage one in 95% fetal bovine serum + 5% DMSO (MEF freezing media). For subsequent use, MEFs were thawed at 37 °C, cultured in MEF media, and incubated at 37 °C with 5% CO_2.

Live cell imaging

2 × 10^4 MEFs were seeded in a Nunc glass-bottomed dish (#150680; Thermo Scientific, Waltham, MA, USA) and cultured overnight in MEF media. The following day, MEF media was replaced with imaging media (DMEM without phenol red + HEPES +10% fetal bovine serum +1% Penicillin/Streptomycin +0.5 μg·mL^{-1} Fungizone) that was incubated overnight at 37 °C with 5% CO_2. Dishes were then sealed with vacuum grease and a glass coverslip. Cells were then imaged every 10 min for 4 h using a 10×/NA0.35 objective with phase contrast illumination on a DeltaVision personalDV in an environmental chamber maintained at 37 °C. Individual cell migration was tracked using the Manual Tracking plugin for ImageJ (National Institutes of Health, Bethesda, MD, USA, version 1.52p) The resulting xy track data was analyzed using the DiPer Excel Macro package [39]. Cells that were multinucleate, divided, or came in contact with other cells were excluded from analysis.

qRT-PCR

WT and *Actb*$^{c\text{-}g}$ isoactin control constructs were generated, and respective primer sets were verified previously [10,40]. An *Actg1*$^{c\text{-}b}$ control construct was generated using site-directed mutagenesis with the QuikChange II XL kit (Cat# 200521; Agilent Technologies, Santa Clara, CA, USA) according to the manufacturer's protocols from the WT pENTR/D-TOPO-*Actg1* vector generated in [40]. New *Actg1* and *Actg1*$^{c\text{-}b}$ specific primers were designed and tested for amplification of all control constructs to assess

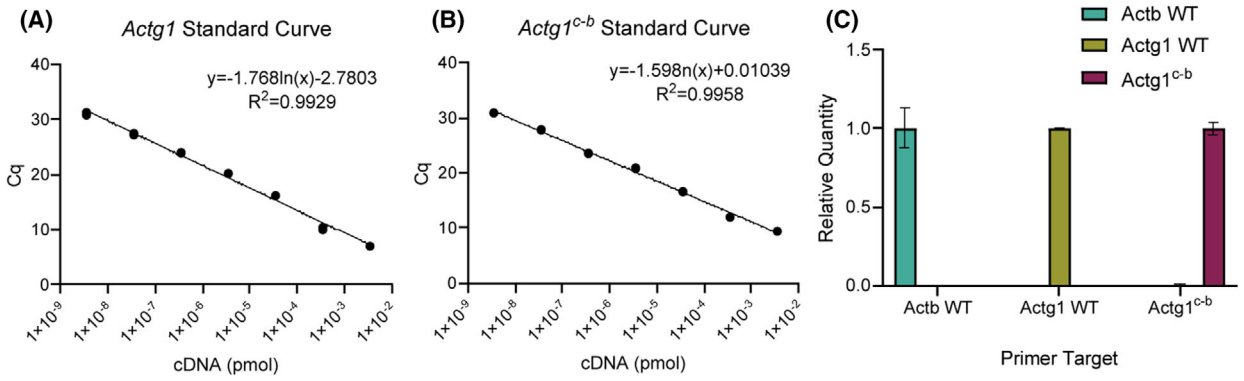

Fig. 9. *Actg1*$^{c\text{-}b}$ qRT-PCR primer specificity and isoform standard curves. (A, B) Representative standard curves generated using new *Actg1* and *Actg1*$^{c\text{-}b}$ primers and control constructs. (C) Representative graph of qRT-PCR primer specificity. $n = 3$; error bars are SEM. Each primer set was used to amplify *Actb*, *Actg1*, and *Actg1*$^{c\text{-}b}$ isoform control constructs to calculate relative quantity. *Actb* and *Actg1* control constructs were generated previously [34]. The x-axis represents the primer target, the y-axis indicates relative quantity, and the colored bars represent amplified Actin isoform.

specificity (Fig. 9). For whole tissue, brains and lungs were pulverized using a mortar and pestle with liquid nitrogen and homogenized in Trizol Reagent (#15596018; ThermoFisher Scientific, Waltham, MA, USA) using a 22G needle and a syringe. Total RNA was extracted from both homogenized tissue and MEFs using the Bio-Rad Aurum Total RNA Mini-Kit (7326820) according to manufacturer's instructions. A NanoDrop 1000 spectrophotometer (ThermoFisher Scientific) was used to measure RNA concentration. First-strand cDNA was generated using the Bio-Rad iScript Advanced cDNA synthesis kit (#1725037) from a standard amount of RNA. A series of 10-fold dilutions of isoactin and *Actg1*$^{c\text{-}b}$ control samples were used to generate standard curves, and MEF or tissue cDNA samples were amplified in parallel using Bio-Rad SsoAdvanced Universal SYBR Green Supermix (1725270) and isoform-specific primers using the Bio-Rad CFX96 Real-Time System C1000 touch thermal cycler. qRT-PCR primers: *Actg1*$^{c\text{-}b}$ forward primer – 5′-TGACGATAGCGCCG CACTCGTCGTC-3′, *Actg1* exon 2 WT forward primer – 5′-AGAAGAAAGCGCCGCACTAGTCATT-3′, *Actg1*/*Actg1*$^{c\text{-}b}$ dual reverse primer – 5′-GCGTCGTCGCCAG CAAAGC-3′.

Western blotting

Brain and lung tissues were pulverized in liquid nitrogen using a mortar and pestle. Brain, lung, and MEF protein were extracted using 1% SDS lysis buffer in 1× PBS with a protease inhibitor mix containing 100 μM aprotinin, 0.79 mg·mL^{-1} benzamide, 1 μM calpain, 1 μM calpeptin, 10 μM E-64, 10 μM leupeptin, and 0.1 mg·mL^{-1} pepstatin, and 1 mM phenylmethylsulfonyl fluoride. MEF lysates were sonicated using an ultrasonic homogenizer (Model 150 V/T; BioLogics Inc., Manassas, VA, USA) and all samples were boiled at 100 °C for 10 min and centrifuged to remove the insoluble fraction. Pulverized gastrocnemius muscle was subjected to low-salt extraction and DNase enrichment as described previously [15]. Equal amounts of cleared lysate were separated by SDS-polyacrylamide gel electrophoresis (SDS/PAGE), transferred to a PVDF membrane, and blocked in 5% nonfat milk in PBS. The following antibodies were used: β-actin (1:5000; Sigma-Aldrich, AC15, Burlington, MA, USA), γ-actin (1:5000 mAB 2–4), α_{sm}-actin (1:5000; Sigma-Aldrich, 1A4, Burlington, MA, USA), Pan-actin (1:5000; Seven Hills Bioreagents, C4, Cincinnati, OH, USA), SRF (1:1000; Santa Cruz Biotechnology, G-20, Dallas, TX, USA), MRTF-A (1:1000; Cell Signaling Technology, E2V2I, Danvers, MA, USA), or YAP (1:500, Abnova, 2F12) with glyceraldehyde 3-phosphate dehydrogenase (GAPDH; 1:5000; Sigma-Aldrich, G9545, Burlington, MA, USA) as a loading control and secondary antibodies DyLight 800 anti-mouse IgG (1:10 000; Cell Signaling Technology, 5257S, Danvers, MA, USA) and DyLight 680 anti-rabbit IgG (1:10 000; Cell Signaling Technology, 5366S, Danvers, MA, USA). Blots were imaged using the Odyssey CLx infrared scanner (LI-COR Biosciences, Lincoln, NE, USA) and protein bands were quantified using LI-COR Image Studio Software as described previously [14].

Open field activity assay

Mice were placed in an open-field apparatus for 15 min, and total vertical movement counts and horizontal distance traveled were measured based on infrared beam breaks, as described in [10]. Activity was measured using the AccuScan system (Columbus Instruments, Columbus, OH, USA).

Ex vivo EDL force measurements

Contractile function of EDL muscles was assessed according to methods described previously [14,41]. Sodium

pentobarbital was used to anesthetize mice (75–100 mg/kg body mass) before dissecting the EDL muscles and mounting them on a 300B-LR dual-mode muscle lever system (Aurora Scientific) using 5–0 suture in a 1.2-mL bath assembly containing oxygenated (95:5% O_2/CO_2) Krebs Ringer bicarbonate (Krebs) buffer maintained at 25 °C. A KPCI-3108 interface board (Keithley Instruments) and TestPoint software (SuperLogics) were used to control the muscle lever and stimulator system. Muscles were adjusted to their anatomical optimal length (L_o) based on resting tension, with length being measured from the distal myotendinous junction to the proximal myotendinous junction using digital calipers. Muscles were stimulated to contract for 200 ms at 175 Hz, and maximal isometric tetanic force (P_o) was measured every 2 min until force plateaued.

Auditory brainstem response

Mice auditory brainstem response (ABR) waveforms were collected using a Tucker Davis Technologies System 3 at frequencies of 4, 8, 11, 16, 22, and 32 kHz as described previously [10]. Subdermal electrodes were used to record scalp potentials following anesthetization with Avertin. Waveforms for each frequency were collected starting at 90 dB, decreasing in 5-dB steps to a subthreshold level. The collected waveforms were stacked, and the lowest level of stimulation that resulted in a definite waveform was considered to be the threshold.

Scanning electron microscopy

Samples were prepared for scanning electron microscopy as previously described [14,25]. Briefly, cochleae were dissected and fixed in 2.5% glutaraldehyde, 0.1 M sodium cacodylate, 2 mM $CaCl_2$ overnight at 4 °C and then decalcified in 170 mM EDTA in PBS for 16 h at 4 °C. Dissected organ of Corti was incubated in 2% each of arginine, glutamine, glycine, and sucrose in water overnight at RT, followed by incubation in 2% tannic acid and guanidine hydrochloride for 2 h at RT, with extensive water washes between steps. The samples were transitioned to 100% ethanol, critical point dried from CO_2, and sputter-coated with gold. Samples were imaged using a JEOL JSM-7800F field emission scanning electron microscope.

Statistics

GraphPad Prism Software (version 10.0.2) was used to conduct all statistical analyses. One- or two-way ANOVAs with Bonferroni posttests were performed based on the specific data set, and significance was determined with $*P < 0.05$, $**P < 0.01$, $***P < 0.001$, and $****P < 0.0001$. SuperPlots were generated as described in [42].

Acknowledgements

This work was supported by NIH Grant T32-AG029796 to LJS, R01-AR049899 to JME, and R01-DC015495 to BJP.

Conflict of interest

The authors declare no conflicts of interest.

Author contributions

LJS planned and performed experiments, analyzed data, and wrote and reviewed the manuscript. KMH performed experiments and analyzed data. JP, WMS, and EEJ performed experiments. XP conceptualized research and planned experiments. BJP and JME conceptualized research, oversaw experimentation and interpretation of results, and wrote and reviewed the manuscript.

Peer review

The peer review history for this article is available at https://www.webofscience.com/api/gateway/wos/peer-review/10.1111/febs.70075.

Data availability statement

The data that support the findings of this study are available from the corresponding authors upon reasonable request.

References

1 Pollard TD & Cooper JA (2009) Actin, a central player in cell shape and movement. *Science* **326**, 1208–1212. doi: 10.1126/science.1175862

2 Morell RJ, Friderici KH, Sainan W, Elfenbein JL, Friedman TB & Fisher RA (2000) A new locus for late-onset, progressive, hereditary hearing loss DFNA20 maps to 17q25. *Genomics* **63**, 1–6. doi: 10.1006/GENO.1999.6058

3 van Wijk E, Krieger E, Kemperman MH, De Leenheer EMR, Huygen PLM, Cremers CWRJ, Cremers FPM & Kremer H (2003) A mutation in the gamma actin 1 (ACTG1) gene causes autosomal dominant hearing loss (DFNA20/26). *J Med Genet* **40**, 879–884. doi: 10.1136/JMG.40.12.879

4 Zhu M, Yang T, Wei S, DeWan AT, Morell RJ, Elfenbein JL, Fisher RA, Leal SM, Smith RJH & Friderici KH (2003) Mutations in the γ-actin gene (ACTG1) are associated with dominant progressive deafness (DFNA20/26). *Am J Hum Genet* **73**, 1082–1091. doi: 10.1086/379286

5 Prins KW, Call JA, Lowe DA & Ervasti JM (2011) Quadriceps myopathy caused by skeletal muscle-specific ablation of Bcyto-actin. *J Cell Sci* **124**, 951–957. doi: 10.1242/JCS.079848
6 Yates TM, Turner CL, Firth HV, Berg J & Pilz DT (2017) Baraitser-winter Cerebrofrontofacial syndrome. *Clin Genet* **92**, 3–9. doi: 10.1111/CGE.12864
7 Parker F, Baboolal TG & Peckham M (2020) Actin mutations and their role in disease. *Int J Mol Sci* **21**, 3371. doi: 10.3390/ijms21093371
8 Perrin BJ & Ervasti JM (2010) The actin gene family: function follows isoform. *Cytoskeleton* **67**, 630. doi: 10.1002/CM.20475
9 Vedula P, Kurosaka S, Leu NA, Wolf YI, Shabalina SA, Wang J, Sterling S, Dong DW & Kashina A (2017) Diverse functions of homologous actin isoforms are defined by their nucleotide, rather than their amino acid sequence. *eLife* **6**, e31661. doi: 10.7554/eLife.31661
10 Patrinostro X, Roy P, Lindsay A, Chamberlain CM, Sundby LJ, Starker CG, Voytas DF, Ervasti JM & Perrin BJ (2018) Essential nucleotide- and protein-dependent functions of Actb/β-actin. *Proc Natl Acad Sci USA* **115**, 7973–7978. doi: 10.1073/pnas.1807895115
11 Sundby LJ, Southern WM, Sun J, Patrinostro X, Zhang W, Yong J & Ervasti JM (2024) Deletion of exons 2 and 3 from Actb and cell immortalization Lead to widespread, β-actin independent alterations in gene expression associated with cell cycle control. *Eur J Cell Biol* **103**, 151397. doi: 10.1016/J.EJCB.2024.151397
12 Vedula P, Fina ME, Bell BA, Nikonov SS, Kashina A & Dong DW (2023) β-Actin is essential for structural integrity and physiological function of the retina. *BioRxiv* doi: 10.1101/2023.03.27.534392
13 Belyantseva IA, Perrin BJ, Sonnemann KJ, Zhu M, Stepanyan R, McGee J, Frolenkov GI, Walsh EJ, Friderici KH, Friedman TB *et al.* (2009) γ-Actin is required for cytoskeletal maintenance but not development. *Proc Natl Acad Sci USA* **106**, 9703–9708. doi: 10.1073/pnas.0900221106
14 Sundby LJ, Southern WM, Hawbaker KM, Trujillo JM, Perrin BJ & Ervasti JM (2022) Nucleotide- and protein-dependent functions of Actg1. *Mol Biol Cell* **33**, ar77. doi: 10.1091/mbc.E22-02-0054
15 Hanft LM, Rybakova IN, Patel JR, Rafael-Fortney JA & Ervasti JM (2006) Cytoplasmic γ-actin contributes to a compensatory remodeling response in dystrophin-deficient muscle. *Proc Natl Acad Sci USA* **103**, 5385–5390. doi: 10.1073/pnas.0600980103
16 Jaeger MA, Sonnemann KJ, Fitzsimons DP, Prins KW & Ervasti JM (2009) Context-dependent functional substitution of α-skeletal actin by γ-cytoplasmic actin. *FASEB J* **23**, 2205–2214. doi: 10.1096/fj.09-129783
17 Bunnell TM & Ervasti JM (2010) Delayed embryonic development and impaired cell growth and survival in Actg1 null mice. *Cytoskeleton* **67**, 564–572. doi: 10.1002/cm.20467
18 Bunnell TM, Burbach BJ, Shimizu Y & Ervasti JM (2011) β-Actin specifically controls cell growth, migration, and the G-actin Pool. *Mol Biol Cell* **22**, 4047–4058. doi: 10.1091/mbc.E11-06-0582
19 Vartiainen MK, Guettler S, Larijani B & Treisman R (2007) Nuclear actin regulates dynamic subcellular localization and activity of the SRF cofactor MAL. *Science* **316**, 1749–1752. doi: 10.1126/SCIENCE.1141084
20 Olson EN & Nordheim A (2010) Linking actin dynamics and gene transcription to drive cellular motile functions. *Nat Rev Mol Cell Biol* **11**, 353–365. doi: 10.1038/nrm2890
21 Baarlink C, Wang H & Grosse R (2013) Nuclear actin network assembly by Formins regulates the SRF coactivator MAL. *Science* **340**, 864–867. doi: 10.1126/SCIENCE.1235038
22 Esnault C, Stewart A, Gualdrini F, East P, Horswell S, Matthews N & Treisman R (2014) Rho-actin signaling to the MRTF coactivators dominates the immediate transcriptional response to serum in fibroblasts. *Genes Dev* **28**, 943–958. doi: 10.1101/GAD.239327.114
23 Seo J & Kim J (2018) Regulation of hippo signaling by actin remodeling. *BMB Rep* **51**, 151–156. doi: 10.5483/BMBRep.2018.51.3.012
24 Sonnemann KJ, Fitzsimons DP, Patel JR, Liu Y, Schneider MF, Moss RL & Ervasti JM (2006) Cytoplasmic γ-actin is not required for skeletal muscle development but its absence leads to a progressive myopathy. *Dev Cell* **11**, 387–397. doi: 10.1016/j.devcel.2006.07.001
25 Perrin BJ, Sonnemann KJ & Ervasti JM (2010) β-Actin and γ-actin are each dispensable for auditory hair cell development but required for Stereocilia maintenance. *PLoS Genet* **6**, e1001158. doi: 10.1371/journal.pgen.1001158
26 Cheever TR, Olson EA & Ervasti JM (2011) Axonal regeneration and neuronal function are preserved in motor neurons lacking ß-actin in vivo. *PLoS One* **6**, e17768. doi: 10.1371/JOURNAL.PONE.0017768
27 Cheever TR, Li B & Ervasti JM (2012) Restricted morphological and behavioral abnormalities following ablation of β-actin in the brain. *PLoS One* **7**, e32970. doi: 10.1371/journal.pone.0032970
28 Shawlot W, Deng JM, Fohn LE & Behringer RR (1998) Restricted β-galactosidase expression of a Hygromycin-LacZ gene targeted to the β- actin locus and embryonic lethality of β-actin mutant mice. *Transgenic Research* **7**, 95–103. doi: 10.1023/A:1008816308171
29 Shmerling D, Danzer CP, Mao X, Boisclair J, Haffner M, Lemaistre M, Schuler V, Kaeslin E, Korn R, Bürki

K *et al*. (2005) Strong and ubiquitous expression of transgenes targeted into the β-actin locus by Cre/lox cassette replacement. *Genesis* **42**, 229–235. doi: 10.1002/GENE.20135

30 Nietmann P, Kaub K, Suchenko A, Stenz S, Warnecke C, Balasubramanian MK & Janshoff A (2023) Cytosolic actin isoforms form networks with different rheological properties that indicate specific biological function. *Nat Commun* **14**, 1–14. doi: 10.1038/s41467-023-43653-w

31 van Zwam MC, Dhar A, Bosman W, van Straaten W, Weijers S, Seta E, Joosten B, van Haren J, Palani A & van den Dries K (2024) IntAct: a nondisruptive internal tagging strategy to study the organization and function of actin isoforms. *PLoS Biol* **22**, e3002551. doi: 10.1371/JOURNAL.PBIO.3002551

32 Chen A, Arora PD, McCulloch CA & Wilde A (2017) Cytokinesis requires localized b-actin filament production by an actin isoform specific nucleator. *Nat Commun* **8**, 1–11. doi: 10.1038/s41467-017-01231-x

33 Chen A, Ulloa Severino L, Panagiotou TC, Moraes TF, Yuen DA, Lavoie BD & Wilde A (2021) Inhibition of polar actin assembly by astral microtubules is required for cytokinesis. *Nat Commun* **12**, 1–13. doi: 10.1038/s41467-021-22677-0

34 Shah R, Panagiotou TC, Cole GB, Moraes TF, Lavoie BD, McCulloch CA & Wilde A (2024) The DIAPH3 linker specifies a β-actin network that maintains RhoA and myosin-II at the Cytokinetic furrow. *Nat Commun* **15**, 1–17. doi: 10.1038/s41467-024-49427-2

35 Heissler SM & Chinthalapudi K (2025) Structural and functional mechanisms of actin isoforms. *FEBS J* **292**, 468–482. doi: 10.1111/FEBS.17153

36 Zhang DS, Piazza V, Perrin BJ, Rzadzinska AK, Poczatek JC, Wang M, Prosser HM, Ervasti JM, Corey DP & Lechene CP (2012) Multi-isotope imaging mass spectrometry reveals slow protein turnover in hair-cell Stereocilia. *Nature* **481**, 520–524. doi: 10.1038/nature10745

37 Narayanan P, Chatterton P, Ikeda A, Ikeda S, Corey DP, Ervasti JM & Perrin BJ (2015) Length regulation of mechanosensitive Stereocilia depends on very slow actin dynamics and filament-severing proteins. *Nat Commun* **6**, 1–8. doi: 10.1038/ncomms7855

38 Drummond MC, Barzik M, Bird JE, Zhang DS, Lechene CP, Corey DP, Cunningham LL & Friedman TB (2015) Live-cell imaging of actin dynamics reveals mechanisms of Stereocilia length regulation in the inner ear. *Nat Commun* **6**, 1–10. doi: 10.1038/ncomms7873

39 Gorelik R & Gautreau A (2014) Quantitative and unbiased analysis of directional persistence in cell migration. *Nat Protoc* **9**, 1931–1943. doi: 10.1038/nprot.2014.131

40 Patrinostro X, O'Rourke AR, Chamberlain CM, Moriarity BS, Perrin BJ & Ervasti JM (2017) Relative importance of βcyto-and γcyto-actin in primary mouse embryonic fibroblasts. *Mol Biol Cell* **28**, 771–782. doi: 10.1091/mbc.E16-07-0503

41 Moran AL, Warren GL & Lowe DA (2005) Soleus and EDL muscle contractility across the lifespan of female C57BL/6 mice. *Exp Gerontol* **40**, 966–975. doi: 10.1016/j.exger.2005.09.005

42 Lord SJ, Velle KB, Mullins RD & Fritz-Laylin LK (2020) SuperPlots: communicating reproducibility and variability in cell biology. *J Cell Biol* **219**, e202001064. doi: 10.1083/jcb.202001064